Characterization of Patient-Derived *GNAQ* Mutated Endothelial Cells from Capillary Malformations

JIDOpen

Ginger Beau Langbroek[1,2,9], Merel L.E. Stor[2,9], Vera Janssen[3], Annett de Haan[3], Sophie E.R. Horbach[2], Mariona Graupera[4,5,6], Carel J.M. van Noesel[7], Chantal M.A.M. van der Horst[2], Albert Wolkerstorfer[8,10] and Stephan Huveneers[3,10]

Capillary malformations (CM) (port-wine stains) are congenital skin lesions that are characterized by dilated capillaries and postcapillary venules. CMs are caused by altered functioning of the vascular endothelium. Somatic genetic mutations have predominantly been identified in the endothelial cells of CMs, providing an opportunity for the development of targeted therapies. However, there is currently limited in-depth mechanistic insight into the pathophysiology and a lack of preclinical research approaches. In a monocenter exploratory study of 17 adult patients with CMs, we found somatic sequence variants in the *GNAQ* (p.R183Q, p.R183G, or p.Q209R) or *GNA11* (p.R183C) genes. We applied an endothelial-selective cell isolation protocol to culture primary endothelial cells from skin biopsies from these patients. We successfully expanded patient-derived cells in culture in 3 of the 17 cases while maintaining endothelial specificity as demonstrated by vascular endothelial-cadherin immunostainings. In addition, we tested the angiogenic capacity of endothelial cells from a patient with a *GNAQ* (p.R183G) sequence substitution. These proof-of-principle results reveal that primary cells isolated from CMs may represent a functional research model to investigate the role of endothelial somatic mutations in the etiology of CMs, but improved isolation and culture methodologies are urgently needed to advance the field.

Keywords: Angiogenesis, Endothelial cells, Port-wine stains, Sturge-Weber syndrome, Vascular malformations

Journal of Investigative Dermatology (2023) ■, ■–■; doi:10.1016/j.jid.2023.10.033

INTRODUCTION

Capillary malformations (CMs), also known as port-wine stains, are congenital vascular lesions affecting the skin and sometimes the underlying tissues. Their typical appearance as red or purple skin stains is caused by hyperdilated capillaries and postcapillary venules (Mulliken et al, 2013; Schneider et al, 1988). Sporadically, spontaneous bleeding may occur, and patients may develop nodules or (bone/soft tissue) overgrowth, which could lead to tissue asymmetry and dysmorphosis (Enjolras and Mulliken, 1993; Geronemus and Ashinoff, 1991; van Drooge et al, 2012). Furthermore, CMs can instigate significant psychological burdens, resulting in a decreased health-related QOL, particularly when lesions are located visibly in the face (Lanigan and Cotterill, 1989; Masnari et al, 2012). In genetic disorders such as Sturge-Weber and Klippel-Trenaunay syndrome, CMs may be accompanied by glaucoma and epilepsy, soft tissue and/or bone hypertrophy, and venous malformations (Lee et al, 2005; Thomas-Sohl et al, 2004). Currently, no cure has been found yet for CMs, and complete vascular normalization is seldom achieved. The current gold standard for treatment is laser therapy, yet despite technological advancements, treatment outcomes in terms of lesional lightening are still not optimal, and lesions recur frequently (Huikeshoven et al, 2007; van Raath et al, 2019).

There is currently a lack of understanding of the molecular and cellular mechanisms that drive CM pathogenesis, although somatic and germline mutations are often found in the endothelial cells of CMs (Nguyen et al, 2019). Specifically, in patients with CMs, recurrent somatic pathogenic variants have been detected in the *GNAQ* gene, *GNA11* gene, and *PIK3CA* gene, and germline mutations have been found in *RASA1* gene (Couto et al, 2017, 2016; Eerola et al, 2003; Revencu et al, 2008; Shirley et al, 2013; Siegel et al, 2018; Vahidnezhad et al, 2016). These genes encode for

[1]*Department of Surgery, Amsterdam Cardiovascular Sciences, Amsterdam UMC, University of Amsterdam, Amsterdam, The Netherlands;* [2]*Department of Plastic, Reconstructive, and Hand Surgery, Amsterdam Cardiovascular Sciences, Amsterdam Public Health, Amsterdam UMC, University of Amsterdam, Amsterdam, The Netherlands;* [3]*Department of Medical Biochemistry, Amsterdam Cardiovascular Sciences, Amsterdam UMC, University of Amsterdam, Amsterdam, The Netherlands;* [4]*Endothelial Pathobiology and Microenvironment, Josep Carreras Leukaemia Research Institute, Barcelona, Spain;* [5]*Institució Catalana de Recerca i Estudis Avancats (ICREA), Barcelona, Spain;* [6]*CIBERONC, Instituto de Salud Carlos III, Madrid, Spain;* [7]*Molecular Diagnostics Division, Department of Pathology, Amsterdam UMC, University of Amsterdam, Amsterdam, The Netherlands; and* [8]*Amsterdam Department of Dermatology, Amsterdam Institute for Infection and Immunity, Amsterdam UMC, University of Amsterdam, Amsterdam, The Netherlands*

[9]*These authors contributed equally to this work.*

[10]*These authors contributed equally to this work.*

Correspondence: Stephan Huveneers, Department of Medical Biochemistry, Amsterdam UMC, location AMC, University of Amsterdam, Meibergdreef 9, 1105 AZ Amsterdam, The Netherlands. E-mail: s.huveneers@amsterdamumc.nl

Abbreviations: CM, capillary malformation; EGM2, Endothelial Cell Growth Medium 2; FCS, fetal calf serum

Received 5 April 2023; revised 12 October 2023; accepted 28 October 2023; accepted manuscript published online XXX; corrected proof published online XXX

Table 1. Patient Eligibility Criteria

Inclusion Criteria	Exclusion Criteria
Adult patients (aged >17 y) of any sex with a CM	Patients with a CM aged <17 y
CMs of all anatomical locations, except facial CMs not extending in the hairline	Facial CMs not extending into the hairline
CMs as part of the Sturge-Weber syndrome	Mix of vascular malformation
	Known coagulation disorders leading to prolonged bleeding
	Anticoagulant use (excluding NSAIDs)
	Cognitively impaired patients

Abbreviations: CM, capillary malformation; NSAID, nonsteroidal anti-inflammatory drug.

proteins central to molecular signaling pathways that when activated, drive cellular growth, proliferation, and survival. The mutations in these genes may lead to modified endothelial cell proliferation, differentiation, survival, and inflammatory status (Huang et al, 2022; Nguyen et al, 2019; Shirley et al, 2013). Confirmatory, at a cellular level, CMs are characterized by hyperactive and proliferative endothelial cells, enlarged vessel lumens, and disorganized perivascular cells (Couto et al, 2016; Le Cras et al, 2020; Nguyen et al, 2019). However, it is still unclear whether and how the genetic mutations lead to vascular lesions and whether targeting the pathways downstream of these genetic variants may cure CMs. With this exploratory prospective study, we aimed to address the functional aspects of primary endothelial cells with genetic sequence substitutions, isolated from CM skin lesions of patients.

RESULTS

Patient characteristics

On the basis of the appointment lists of the outpatient clinic at the Department of Dermatology (Amsterdam UMC, Amsterdam, The Netherlands), a total of 59 potentially eligible patients with CM were identified. By screening the electronic patient files, 24 patients (41%) were considered not eligible on the basis of the predefined exclusion criteria (Table 1). The remaining 35 patients (59%) were subsequently contacted to participate. Of these patients, eventually, 17 patients (49%) agreed to participate in this study, and skin biopsies were taken accordingly.

Table 2 lists all patient characteristics. Most patients were female (76%, n = 13), the mean age was 35 years (SD ± 17 years), and Fitzpatrick type 2 was the most frequent skin type (76%, n = 13). The majority of the patients had a CM in the head and neck region (76%, n = 13). Local hypertrophy, including blebs, was present in 8 patients (47%), and soft tissue overgrowth was present in 9 patients (53%). Telangiectasia was found in only 3 patients (18%). A total of 13 patients had another laser therapy session planned after the biopsies were taken; the mean time to follow-up was 16 weeks (SD ± 4).

Genetic and histological analysis

By sequencing the CM biopsies, we detected somatic sequence substitutions in 13 patients (76%): the *GNAQ* gene was mutated in 11 patients (85%), and the *GNA11* gene was mutated in 2 patients (15%). The detected allele frequency of the point mutations ranged between 2 and 15% within the lesions, with a mean of 8.2%. The most predominant somatic sequence substitution was the *GNAQ* (c.548G>A; p.R183Q) (n = 8), confirming previous findings (Shirley et al, 2013). Moreover, we identified the *GNAQ* (c.626A>G; p.Q209R) mutations in 2 patients, 1 *GNAQ* (c.547C>G; p.R183G) mutation, and 2 patients with a *GNA11* (c.547C>T; p.R183C) mutation. In 4 patients, no pathogenic sequence variant was found. In this study, we did not observe a clear genotype–phenotype correlation between CM characteristics and somatic mutations. Histological analysis of the CM coupes showed enlarged vessel lumens in the skin specimens (Figure 1a). In addition, we observed vascular leakage in a patient with lesions containing a *GNAQ* (c.626A>G; p.Q209R) sequence substitution (biopsy 5).

Isolation and expansion of patient-derived primary endothelial cells

Recently, an endothelial cell isolation protocol was successfully developed for low-flow vascular malformations (Kobialka et al, 2022). To assess the possibility of obtaining primary cells from the lesions of patients with CM lesions, we aimed to isolate and expand cells from the 4-mm biopsies of the patient cohort. Fresh surgical biopsies of CMs were tissue digested, and endothelial cells were purified from the homogenate by using anti-CD31–conjugated magnetic beads as described before for *PIK3CA*-related vascular malformations (Kobialka et al, 2022). The remaining cell fractions were taken into culture to expand patient-derived primary skin fibroblasts. Initially, the CD31-enriched cell fraction formed small colonies that in the course of 2–4 weeks grew into cobblestone-shaped monolayers, a typical characteristic of cultured endothelial cells (Figure 1b). Of note, during tissue culture expansion, 5 patient-derived endothelial lines were lost owing to cell senescence and/or the overgrowth of remaining fibroblasts. Attempts to eradicate fibroblast contaminations from the endothelial cultures through a second CD31-magnetic bead selection step did not fully remove fibroblasts. In addition, some endothelial cultures expanded inefficiently (for instance, biopsy 9 *GNAQ* p.R183Q cells). The size and shape of the proliferating endothelial cells did not differ between CM and healthy tissues, indicating that overall endothelial cell morphology is maintained in CMs. To further investigate the characteristics of the patient-derived cells, we performed immunofluorescence stainings for the endothelial-specific marker vascular endothelial-cadherin, the F-actin cytoskeleton (phalloidin), and the nucleus (DAPI) in the expanding cultures (Figure 2). These immunostainings confirmed that bona fide endothelial monolayers were expanded from patient biopsies harboring a *GNAQ* p.R183Q (biopsies 2 and 8) mutation and *GNAQ* p.R183G (biopsy 6) as well as from the 2 healthy control biopsies.

Angiogenic sprouting capacity of patient-derived *GNAQ* (p.R183G) endothelial cells

The formation of vascular malformations depends on sprouting angiogenesis (Kobialka et al, 2022). Thus far, it has not been possible to assess the function of CM-derived endothelial cells. To functionally test the angiogenic

Table 2. Somatic Sequence Variants and Phenotype Characteristics

Patient Number	Gene	Sequence Variants	VAF	Sex, Age (in y)	Fitzpatrick Skin Type	Color	Anatomic Location	Size (cm)	Tissue Overgrowth	Nodules and Blebs	Telangi-ectasia	Biopsy Site	Time to Follow-Up (wk)
1	*GNAQ*	Exon 4 c.548G>A p.R183Q	8%	Female, 18	Type 2	Red to purple	The left chest	8 × 5.5	No	No	Yes	Border left and right mammae	15
2	*GNAQ*	Exon 4 c.548G>A p.R183Q	11%	Female, 25	Type 2	Light red	Right side of the face (cheek, lips, neck, ear)	20 × 15	Lower lip	No	No	Hairline behind the right ear	N/A[1]
3	*GNA11*	Exon 4 c.547C>T p.R183C	2.05%	Female, 43	Type 2	Light red to red	Left side of the face (skull, orbita, cheek, and lip)	10 × 6	Upper lip	No	No	Hairline left	N/A[1]
4	*GNAQ*	Exon 5 c.626A>G p.Q209R	2.48%	Female, 21	Type 2	Dark red to purple	Chest: left breast toward the left flank	20 × 15	No	No	No	Left flank close to IMF	18
5	*GNAQ*	Exon 5 c.626A>G p.Q209R	11%	Male, 40	Type 2	Dark red	Left side of head: beyond hairline toward ear and neck	6.1 × 3.6	No	Yes	Yes	In hairline	21
6	*GNAQ*	Exon 4 c.547C>G p.R183G	3.68%	Female, 54	Type 3	Red	Left side of the face, above the upper lip, cheek, temporal region, ear, and neck	7 × 15	No	Yes	Yes	Behind left ear	20
7	*GNAQ*	Exon 4 c.548G>A p.R183Q	9%	Male, 30	Type 3	Dark red to purple	Face and neck: lower lip, chin, both cheeks and neck continuing to chest	20 × 30	Chin and lower lip	Yes	No	Right side chest	18
8	*GNAQ*	Exon 4 c.548G>A p.R183Q	7.2%	Female, 19	Type 1	Red and purple	Head and neck: right face continuing in hairline, ear, and neck	15 × 10	Soft tissue right side face zygoma/infraorbital, possibly also bony overgrowth	Yes	No	Behind right ear	12
9	*GNAQ*	Exon 4 c.548G>A p.R183Q	12%	Female, 76	Type 2	Red	Head and neck: left front face continuing into hairline left side	10 × 20	Upper lip and eyebrow left	Yes	No	Frontotemporal left in the hairline Healthy tissue: left upper leg	14
10	*GNAQ*	Exon 4 c.548G>A p.R183Q	2.63%	Female, 26	Type 2	Light red to red	Neck: right anterior of carotid artery	8 × 3	No	No	No	Neck, cranial site of the CM	11
11	Not found	N/A	N/A	Female, 24	Type 4	Red	Head and neck: right front face, upper eyelid, temporal, cheek, and neck	Unreported	Upper and lower lip and supraorbital right	Yes	No	Behind left ear	11
12	Not found	N/A	N/A	Female, 66	Type 2	Red	Head and neck: right side face, nose, lips, and chin continuing in the hairline right	30	Soft tissue overgrowth of upper lip, nose, cheek right	No	No	Preauricular right in the hairline Healthy tissue: right upper arm	N/A[1]
13	*GNA11*	Exon 4 c.547C>T p.R183C	12%	Female, 28	Type 2	Light red	Head and neck, upper and lower extremity left and trunk: complete face, neck, chest left side and left arm and leg	150 × 30	No	No	No	Left upper arm	9

(*continued*)

Table 2. Continued

Patient Number	Gene	Sequence Variants	VAF	Sex, Age (in y)	Fitzpatrick Skin Type	Color	Anatomic Location	Size (cm)	Tissue Overgrowth	Nodules and Blebs	Telangi-ectasia	Biopsy Site	Time to Follow-Up (wk)
14	Not found	N/A	N/A	Male, 38	Type 2	Light red to red	Head and neck: right side front face until midline, both cheeks, temporal region, skull, and neck both sides	15 × 20	No	No	No	Behind right ear	11
15	Not found	N/A	N/A	Female, 37	Type 2	Dark red to purple	Trunk, upper and lower extremity: right arm, half side back right, buttocks both sides, both legs back side	140 × 50	No	Yes	No	Right lower leg laterally	23
16	*GNAQ*	Exon 4 c.548G>A p.R183Q	11%	Male, 36	Type 2	Dark red to purple	Head, neck, trunk: multiple CMs face right into hairline, preauricular, cheek, jawline, and neck. Small CM shoulder/back	25 × 10	Soft tissue overgrowth of the face	Yes	No	Right shoulder/back	N/A[1]
17	*GNAQ*	Exon 4 c.548G>A p.R183Q	15%	Female, 23	Type 2	Light red	Upper extremity and trunk: right side chest to inframammary fold, continuing to back midway. Complete right arm affected.	80 × 80	Soft tissue overgrowth of arm and hand right	No	No	Right upper arm	20

Abbreviations: CM, capillary malformation; IMF, inframammary fold; N/A, not applicable; VAF, variant allele frequency.

The table displays an overview of the somatic sequence variants and associated phenotypic characteristics per patient in this study. No clear phenotypic differences (regarding CM anatomic location, size, tissue overgrowth, nodules/blebs, and telangiectasia) were found between *GNAQ* and *GNA11* sequence variants.

[1]In 4 patients, time to follow-up could not be determined because these patients completed laser therapy, and thus no following laser treatment were scheduled.

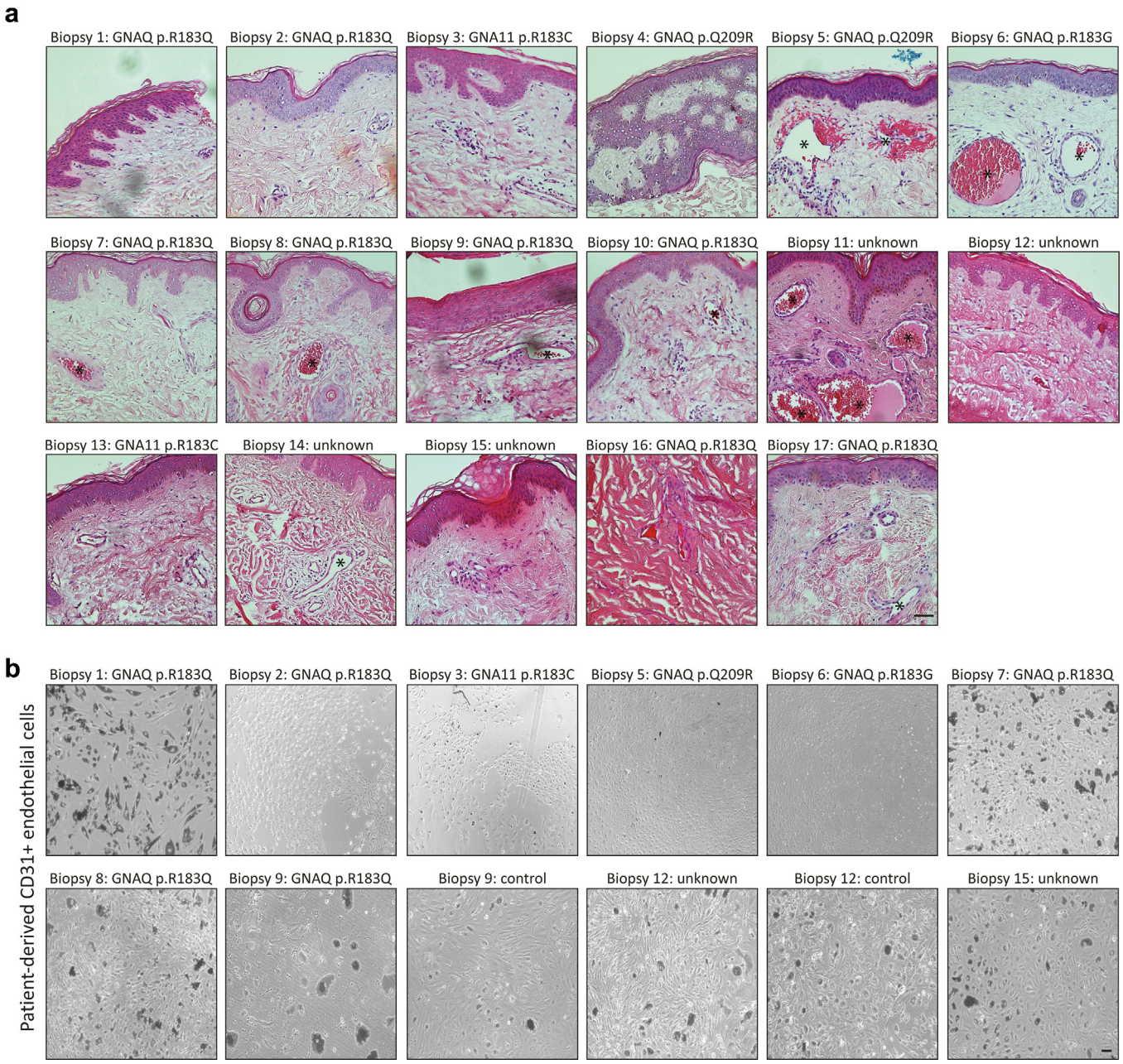

Figure 1. Characterization of skin capillary malformations and patient-derived endothelial cells. (**a**) Bright-field images of H&E-stained tissue section from patient skin. Clear dilated capillaries are visible in biopsy samples 5, 6, 7, 8, 9, 10, 11, 14, and 17 (indicated by *). In addition, there was vascular leakage from the CMs in a *GNAQ* (c.626A>G; p.Q209R)–positive lesion (biopsy 5). Bar = 50 μm. **(b)** Phase-contrast images of patient-derived primary endothelial cell cultures, which were selected by anti-CD31–coated magnetic beads. Black aggregates are the remaining magnetic beads that were used to enrich the endothelial cells from patient tissue. Bars = 50 μm. CM, capillary malformation.

capacity of CM-derived endothelial cells, we first sequenced the DNA of the culture-expanded endothelial cells from biopsy 6, which confirmed the *GNAQ* (c.547C>G; p.R183G) sequence substitution. The allelic frequency of the mutation increased to 20% (from 3.7% in the original CM tissue). The increased variant allele frequency might indicate that the somatic mutation increased the endothelial proliferation rate compared with that in the normal endothelial cells in a mosaic culture or that the mutation is enriched in the endothelial cell isolated fraction. To investigate the angiogenic potential of the CM-derived *GNAQ* p.R183G endothelial cells, we performed angiogenic GF-induced sprouting assays on the basis of endothelial multicellular spheroids in 3-dimensional collagen matrix. The CM-derived *GNAQ* p.R183G endothelial cells could be sufficiently expanded to perform 2 independent assays, showing that these cells are able to sprout (Figure 3a and b). Owing to the limited growth of the other patient-derived endothelial cultures, a comparative analysis of angiogenic sprouting capacity from multiple patients could not be performed. For the same reason, follow-up experiments to assess endothelial barrier function, scratch wound migration, and biochemical signals in lysates could not be executed. Taken together, these results indicate that the angiogenic sprouting capacity of capillary endothelial

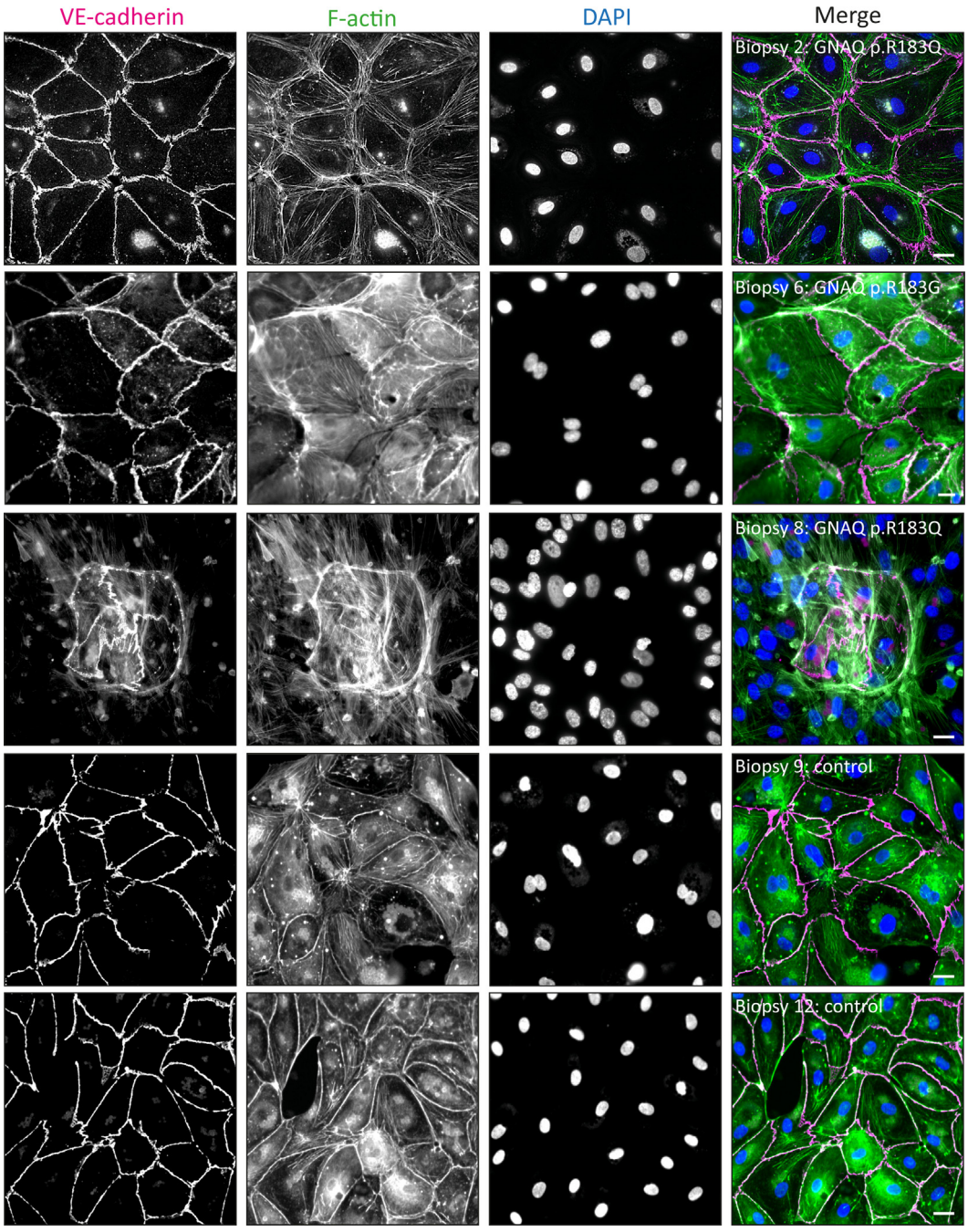

Figure 2. CD31-selected patient-derived cells are endothelial cells. Shown are representative widefield immunofluorescence images taken from culture-expanded CD31-selected patient-derived primary endothelial cell cultures stained for the endothelial marker VE-cadherin (magenta), F-actin cytoskeleton (phalloidin, green), and nucleus (DAPI, blue). Bars = 20 μm. VE-cadherin, vascular endothelial-cadherin.

cells from patients carrying a *GNAQ* p.R183G sequence substitution is retained. A larger study that includes endothelial cells from different patients and from controls such as normal skin is needed to be able to assess the impact of CM-related mutations on angiogenic sprouting capacity.

DISCUSSION

In this study, we showed that primary cells isolated from cutaneous CMs may represent a functional research model to investigate the importance of endothelial somatic mutations in the etiology of CMs. It is expected that future larger studies will define the relevance of specific mutations in the *GNAQ* and *GNA11* genes for the development of cutaneous CMs and related clinical features.

Expansion of patient-derived primary cells

This study indicates that it is possible to isolate and expand primary endothelial cells from CM lesions. The experimental approach enables the identification of key perturbed endothelial functions in CMs and whether such dysfunctions are associated with specific genetic predispositions and/or clinical features. The patient-derived cells are useful as a disease

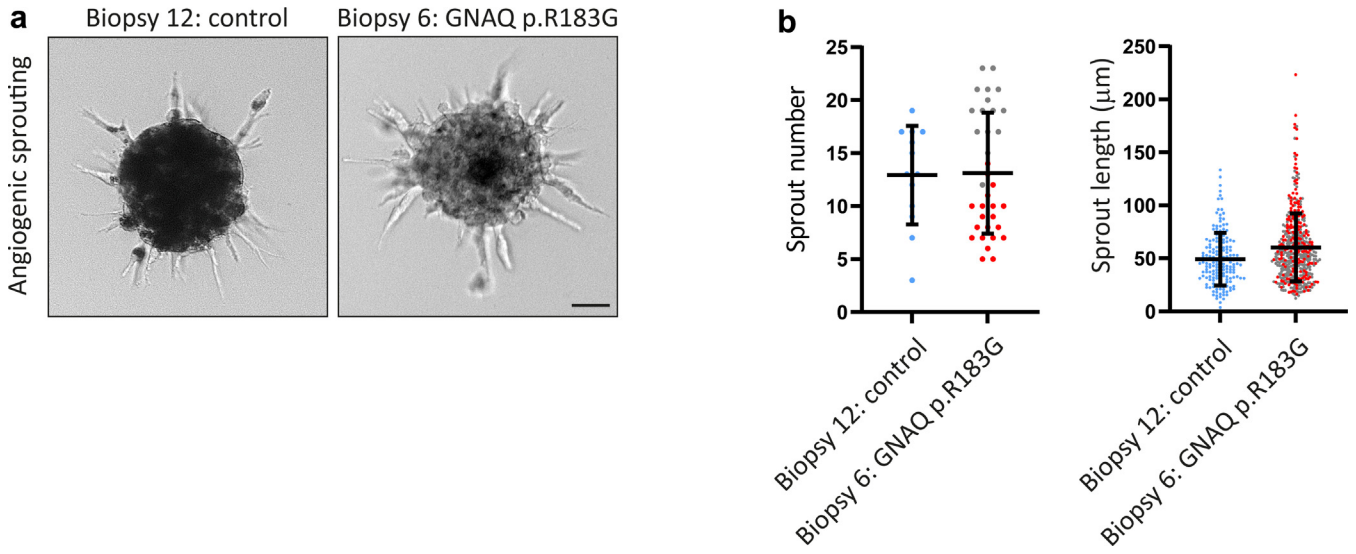

Figure 3. Capillary malformation–derived *GNAQ* p.R183G endothelial cells display increased angiogenic sprouting. (**a**) Representative phase-contrast images of sprouting spheroids 24 hours after VEGF stimulation of patient-derived endothelial cells. The sprouting capacity of control endothelial cells was compared with that of capillary malformation–derived *GNAQ* p.R183G endothelial cells. Bar = 50 μm. (**b**) Graphs show the mean ± SD sprout length and number of sprouts. Data representing n = 13 spheroids from control endothelial cells (from 1 biological replicate) and n = 35 spheroids from *GNAQ* p.R183G endothelial cells (from 2 biological replicates; indicated by distinct colors of the data points in the graph) were analyzed.

model in which the somatic mutations, molecular signaling pathways, and cellular functions from CMs are recapitulated. We expect that the use of patient-derived primary cells, once expanded sufficiently, will spur the development of compound or therapeutic screens that are aimed at restoring endothelial function in CMs. Furthermore, identifying the effector pathways of the mutated genes that underlie CM formation will allow for the potential development of targeted therapies. Our results also indicate that the efficiency of expansion of endothelial cells from CMs is very low, perhaps less efficient than endothelial cells derived from PIK3CA-related vascular malformations (Kobialka et al, 2022), which is coherent with the notion that those lesions are highly proliferative and more associated with tissue overgrowth (Angulo-Urarte and Graupera, 2022). In this study, only the *GNAQ* p.R183G–mutated endothelial cells expanded sufficiently to be able to perform angiogenic-sprouting assays. We posit that the success in expanding the endothelial cells cannot be attributed to specific CM characteristics exhibited by the respective patient. This conclusion is drawn from the observation that the clinical characteristics of the CMs (ie, located in the head and neck region and featuring local blebs) in the other patients were found to be similar and shared commonalities. In addition, the biopsy was taken from the skin behind the ear, which was also a frequent tissue biopsy site in the other patients. Whether the *GNAQ* p.R183Q, *GNAQ* p.Q209R, or *GNA11* p.R183C sequence substitutions have a potential negative impact on endothelial cultures is currently unclear. Expression of the closely related hyperactive *GNAQ* p.Q209L mutation in endothelial cells has been shown to induce vascular malformations in mice (Sasaki et al, 2022; Schrenk et al, 2023), providing proof of principle that mutations in *GNAQ* are disease drivers. Of note, skin biopsies may also be used to expand patient-derived fibroblasts, which is much more efficient in terms of collecting large numbers of cells. These fibroblasts, provided they carry the somatic mutation, can serve as a viable source for generating induced pluripotent stem cells. Endothelial cells, pericytes, and smooth muscle cells can be differentiated from these induced pluripotent stem cells (Orlova et al, 2014; Vila Cuenca et al, 2021) to generate genetically identical CM vascular cell types.

Genetic mutations

Somatic and germline mutations in genes regulating cell growth are known to cause CMs. However, in 4 patients, we were not able to detect any genetic alterations. This might have several reasons: (i) the allele frequency is below the sequencing detection limit, (ii) the mutation is in a gene that was not included in the applied gene panel, or (iii) the mutation is present in another part of the gene. In this study, we most frequently found somatic pathogenic sequence substitutions in the *GNAQ* gene (85%), which is in line with previous findings (Couto et al, 2016; Shirley et al, 2013). *GNA11* was another mutated gene found in some of our included patients. Both genes code for G proteins (ie, Gαq and Gα11), which are part of heterotrimeric G protein complexes that mediate signaling through G-protein–coupled receptors. The somatic mutations induce expression of hyperactive Gαq and Gα11 protein variants (Shirley et al, 2013).

Currently, the presence of clinical distinctions between patients harboring *GNAQ* and *GNA11* sequence substitutions remains uncertain; however, it is notable that *GNAQ* mutations have been closely correlated with facial CMs, whereas *GNA11* mutations have been associated with extremity CMs and tissue overgrowth (Couto et al, 2017, 2016; Lian et al, 2014; Shirley et al, 2013). In addition, a recent study among 32 patients with CMs found that port-wine stains, ipsilateral

segmental overgrowth, varicose veins, and macrocephaly were associated with *GNAQ* sequence variants, whereas cutis marmorata, nevus anemicus, and ipsilateral hypotrophy were associated with *GNA11* sequence variants (Jordan et al, 2020). Owing to the low number of patients with *GNA11* sequence substitutions (n = 2) in this study, we were not able to establish phenotypic differences between *GNAQ* and *GNA11* mutations. Somatic sequence variants in *PIK3CA* are widely present in low-flow malformations and overgrowth disorders and also have been recently identified in patients with diffuse multifocal CMs and overgrowth (Goss et al, 2020). Finally, CMs have been associated with germline *RASA1* and *EPHB4* sequence variants, resulting in a phenotype with multiple, round-to-oval, pink, hereditary CMs, some with a pale halo (Amyere et al, 2017; Revencu et al, 2013). Patients included in this study did not portray these phenotypic descriptions, and no *RASA1* or *EPHB4* sequence variants were identified in this patient cohort. Future larger-scale studies are needed to investigate how mutations in the *GNAQ* and *GNA11* genes contribute to the development of CMs and associated clinical features in patients and explore possible genotype–phenotype correlations.

Patient study limitations

Several limitations to this study need to be mentioned. First, the number of samples was small owing to the exploratory character of this case series, which prevented comparative statistical analysis, and thus no correlations could be made between patient phenotype and genotype. The initial sample size was decided arbitrarily on the basis of the limited availability of funding for the genetic analysis and cellular experiments. Owing to the COVID-19 pandemic and rarity of the disease, the inclusion rate was slow, after which it was decided to stop inclusion at n = 17 participants. Second, selection bias in this study cannot be fully ruled out because only patients who opted for laser therapy for their CM were included. Therefore, more severely affected patients with larger and thicker CMs or in highly visible areas, such as the head and neck region, could be overrepresented. Third, to be able to definitively conclude whether a somatic sequence substitution leads to a different cellular phenotype, paired control cells should be compared with mutated endothelial cells from the same patient. Therefore, developing approaches that may separate mutated from normal endothelial cells from the biopsies would be preferred. Finally, we were only able to assess angiogenic-sprouting capacities in endothelial cells from 1 patient in 2 biological replicates because the cells of the majority of the patients did not continue to proliferate in culture. An innovative experimental protocol was applied for the derivation of endothelial cells for which no practical guideline is yet available. To improve the expansion of patient-derived endothelial cells, culture protocol optimizations may be required. The addition of more GFs—in this study, we increased fetal calf serum (FCS) to 12% in the culture medium—already improved the expansion of the primary cultures. Alternatively, CD31-selected cells from biopsies may be directly assessed for their sprouting capacity in the angiogenesis assay, provided that the biopsies contain a sufficient number of endothelial cells to generate spheroids. Future studies may focus on identifying and defining essential GFs, which improve the isolation and expansion protocol. This study therefore serves as a practical guide for other researchers aiming to derive endothelial cells from skin biopsies in patients with CM and as a stepping stone for future studies.

In conclusion, our study showed that primary cells isolated from cutaneous CMs are able to expand while maintaining endothelial cell specificity, resulting in a valued research model to assess the endothelial cell function of CMs. Increased angiogenic activity may contribute to CM formation and/or progression. Using patient-derived endothelial cells, we found that endothelial cells from patients carrying a somatic *GNAQ* (R183G) sequence substitution retained angiogenic sprouting capacity. We obtained sufficient endothelial cells from normal skin tissue as control in only 1 of the independent sprouting assays. These preliminary experiments indicate that there was no large difference in the number of induced sprouts in the CM-derived *GNAQ* p.R183G endothelial cells (mean number of sprouts per spheroid = 13.1; SD ± 5.7) compared with that in the control (mean number of sprouts per spheroid = 12.9; SD ± 4.6) (Figure 3a and b). The length of forming sprouts in CM-derived *GNAQ* p.R183G endothelial cells (mean sprout length = 60.3 μm; SD ± 32.0) seemed higher than that in healthy skin-derived endothelial cells from biopsy 12 (mean sprout length = 49.3 μm; SD ± 24.8). These results point toward the possibility that CM-derived *GNAQ* p.R183G endothelial cells may have altered angiogenic sprouting properties. Clearly, stronger evidence is needed to define whether such functional changes underlie the increased number of dilated capillaries in CMs. Future research efforts should focus on the use of patient-derived primary cells in the search for therapeutic treatments that restore endothelial function in CMs.

MATERIALS AND METHODS

Study design

The prospective case series was performed at the Department of Dermatology of a tertiary Vascular Anomalies Center at Amsterdam University Medical Centers (Amsterdam UMC) in Amsterdam, The Netherlands. The STROBE (Strengthening the Reporting of Observational Studies of Epidemiology) checklist for cross-sectional studies was followed (Cuschieri, 2019). The study adhered to the Declaration of Helsinki, and written informed consent was obtained from all patients. The study was approved by the Medical Ethics Committee from the Amsterdam UMC (case number NL75128.018.20), and the study was registered at the National Trial Register in the Netherlands on February 23, 2021 (trial identification NL9295).

Participants

Study participants encompassed adult patients (aged >17 years) with a CM receiving laser therapy at the Department of Dermatology at the Amsterdam UMC, location AMC. CMs of all anatomical locations were eligible for inclusion; in patients with a facial CM, the lesion had to extend into the hairline, so that the tissue biopsy could be taken from a nonvisible site. Patients with a mix of vascular malformations were excluded from this study. Table 1 summarizes all patient eligibility criteria. For this explorative study, the aim was to include 20 patients in total, which was based on estimated patient flow and budgetary constraints.

Study outcomes

Intended study outcomes included the assessment of the histology, biochemical activity profile in endothelial lysates, endothelial barrier function, and angiogenic-sprouting and scratch wound healing capacities of endothelial cells from CMs. Furthermore, we assessed the presence of somatic sequence variants in CMs and explored their correlations with CM phenotypic characteristics.

Data and sample collection

Patients with a CM visiting the outpatient clinic for laser therapy between April 2021 and July 2022 were screened for eligibility. Before the laser sessions, patient and lesion characteristics (ie, sex (male/female), age, Fitzpatrick skin type, previous therapies, lesion size, color, location, presence of soft tissue/bone overgrowth and nodules/blebs, or telangiectasia) were collected. Of each patient, 2 skin tissue biopsies were taken from a not recently lasered area of the CM. Of these tissue biopsies, 1 biopsy of 3 mm in diameter was taken for histological and molecular analysis and preserved in saline until further processing. The second tissue biopsy of 4 mm was taken and preserved in Endothelial Cell Growth Medium 2 (EGM2) complete medium in an incubator at 37 °C before endothelial cell isolation. In addition, a control biopsy of normal skin (4 mm) was taken from 2 patients with CM to enable comparison of cells from CM with those from healthy tissue. Next, laser sessions commenced, and the treatment course occurred as planned. Patients were followed up during their regular appointments for their CM laser treatment (approximately 3−4 months after the last treatment).

Next-generation sequencing for genetic analysis

The 3-mm tissue biopsies were processed for histology, embedded in paraffin, and cut into coupes. Subsequently, DNA was isolated from the coupes using 400 µg proteinase K. The extracted DNA was analyzed with next-generation sequencing for common sequence variants in vascular malformation−associated genes, including the *GNAQ*, *GNA11*, *PIK3CA*, and *RASA1* genes. These sequence variants are known from previously published studies on patients with CMs or vascular tumors (Cai et al, 2019; Couto et al, 2016; Fjær et al, 2021; Jansen et al, 2021; Shirley et al, 2013). Supplementary File S1 shows a complete overview of the applied gene panel.

Histological analysis

CM tissue sections from the 3-mm biopsies were H&E stained. The histological images were assessed by an experienced pathologist and compared with histological images of healthy skin.

Endothelial cell isolation and culture

Endothelial cells were isolated from the 4-mm tissue biopsies on the basis of a previously developed protocol for low-flow vascular malformations (Kobialka et al, 2022). Cells were immediately isolated from the biopsies when obtained (of note, biopsy 15 was stored overnight in EGM2 in an incubator at 37 °C before processing). Biopsies were homogenized using scalpels and incubated with dispase II (0.050 mg/ml; number 04942078001, Roche Diagnostics GmbH) and collagenase A (10 mg/ml; number 10103578001, Roche Diagnostics GmbH) in Hank's Balanced Salt Solution (no magnesium, no phenol red; number 14175053, Gibco) supplemented with penicillin/streptomycin for 1 hour at 37 °C. During the incubation, the sample was vortexed every 10 minutes. Next, the tissue homogenate was mixed by pipetting using a P1000 pipette until aggregates were disintegrated. The sample was filtered over a 40-µm cell strainer and washed with DMEM containing 10% FCS to deactivate the digestive enzymes. The cells were centrifuged at 1200 r.p.m. for 5 minutes (room temperature), resuspended in 5 ml PBS + 0.5% BSA, centrifuged at 1200 r.p.m. for 5 minutes, resuspended in 1-ml PBS + 0.5% BSA and transferred to a 1.5-ml tube, centrifuged at 1200 r.p.m. for 5 minutes, and resuspended in 100-µl PBS + 0.5% BSA. For each biopsy. 6.4×10^6 (16 µl) magnetic Dynabeads (Pan mouse IgG, number 11041, Invitrogen) were washed 5 times in 1-ml PBS + 0.5% BSA and coupled to 2.5 µl anti-CD31 antibody (monoclonal mouse anti-human CD31 clone JC70A, number M0823, Agilent Dako) in 16-µl PBS + 0.5% BSA in low binding Eppendorf tubes for 1 hour at room temperature, protected from light while mixing the beads every 5−10 minutes by gently tapping the bottom of the tube. Beads were resuspended in 100-µl PBS + 0.5% BSA. Next, the bead suspension was added to the isolated cells and incubated for 1 hour, mixed head over head, at room temperature, protected from light. After the incubation, the bead−cell suspension was resuspended in EGM2 and placed on a magnet. The supernatant (CD31−) fraction was taken in culture to obtain skin fibroblasts, and the pellet (CD31+) fraction was resuspended in EGM2 and cultured in 0.5% gelatin-coated 12-well plates. Endothelial cells and fibroblasts were cultured in EGM2 supplemented with growth medium 2 supplement pack (PromoCell) and FCS. Initially, 2% FCS was used, which resulted in slow growth of the primary endothelial cells. As a result, the FCS concentration was adjusted to 12% FCS to improve the growth of endothelial cells.

Immunofluorescence stainings

For immunofluorescence stainings, cells were cultured on 5-µg/ml fibronectin-coated coverslips. Cells were fixed by 10-minute incubation with 4% paraformaldehyde in PBS^{++} (PBS with 1 mM calcium chloride and 0.5 mM magnesium chloride). Fixed cells were permeabilized for 5 minutes with 0.5% Triton X100 in PBS and blocked for 30 minutes in 2% BSA in PBS. Antibody (Alexa Fluor-647−conjugated anti-human vascular endothelial-cadherin, clone 55-7H1, number 561567, BD Biosciences, diluted 1:100) and markers (AlexaFluor 568-phalloidin−diluted 1:1000, number A12380 and DAPI number 1306, diluted 1:1000, were from Invitrogen) were diluted in PBS + 0.5% BSA and incubated for 45 minutes. Stained cells were washed 3 times with PBS + 0.5% BSA, and coverslips were mounted in Mowiol4-88/DABCO solution (Sigma-Adrich).

Microscopy

H&E slides were imaged using a Leica DM6 upright microscope with 20× objective. Cell cultures and sprouting assays were imaged with an EVOS M7000 imaging system using 4× and 10× objectives. Immunofluorescently stained samples were imaged using an inverted NIKON Eclipse TI equipped with a 20x objective, a lumencor SOLA SEII light source, standard DAPI, mCherry and Cy5 filter cubes, and an Andor Zyla 4.2 plus sCMOS camera. Images are enhanced for display using ImageJ.

Sprouting assay

For the VEGF-induced sprouting angiogenesis assay, cells were resuspended in EGM2 medium with 0.1% methylcellulose (4.000 cP, Sigma-Aldrich). Spheroids were formed by seeding 750 cells per 100 µl methylcellulose medium in a 96 U-bottom-wells plate and incubation for 24 hours at 37 °C and 5% carbon dioxide.

Subsequently, spheroids were collected and resuspended in 1.7 mg/ml collagen type I rat tail mixture (number 50201, ibidi) and plated in a glass bottom 96-well plate as described previously (Korff and Augustin, 1999; van der Stoel et al, 2020). After stimulation with 50 ng/ml VEGF to induce sprouting, spheroids were incubated for 24 hours at 37 °C and 5% carbon dioxide. Sprout length was assessed using the ImageJ plugin NeuronJ (Meijering et al, 2004), and sprout number was counted manually.

Statistical analysis

Categorical data are expressed as numbers (n) and percentages (%), and continuous variables are presented as means with SDs. All dot graphs represent the mean ± SD. No statistical tests were performed owing to the lack of sufficient biological replicates.

Data availability statement

No large datasets were generated or analyzed.

ORCIDs

Ginger Beau Langbroek: http://orcid.org/0000-0002-9801-1415
Merel L. E. Stor: http://orcid.org/0000-0002-4331-9631
Vera Janssen: http://orcid.org/0000-0002-0788-8060
Annett de Haan: http://orcid.org/0009-0004-6922-7403
Sophie E. R. Horbach: http://orcid.org/0000-0002-3165-4774
Mariona Graupera: http://orcid.org/0000-0003-4608-4185
Carel J. M. van Noesel: http://orcid.org/0000-0001-7907-7390
Chantal M. A. M. van der Horst: http://orcid.org/0000-0002-4937-3786
Albert Wolkerstorfer: http://orcid.org/0000-0003-1421-1493
Stephan Huveneers: http://orcid.org/0000-0002-1091-475X

CONFLICT OF INTEREST

The authors state no conflict of interests

ACKNOWLEDGMENTS

We thank Cindy van Roomen, the Core Facility Genomics, and the Pathology Department of the Amsterdam University Medical Center for experimental support. This research was financially supported by the Netherlands Organization of Scientific Research (NWO OCENW.KLEIN.281) and the AMC Foundation awarded to SERH.

AUTHOR CONTRIBUTIONS

Conceptualization: GBL, MLES, CMAMvdH, AW, SH; Formal Analysis: GBL, MLES, SERH, CJMvN, AdH, VJ, SH; Investigation: GBL, MLES, AdH, VJ; Methodology: MG; Supervision: CMAMvdH, AW, SH; Writing − Original Draft Preparation: GBL, MLES, VJ, SH; Writing − Review and Editing: GBL, MLES, AdH, VJ, SERH, CJMvN, MG, CMAMvdH, AW, SH

SUPPLEMENTARY MATERIAL

Supplementary material is linked to the online version of the paper at www.jidonline.org, and at https://doi.org/10.1016/j.jid.2023.10.033.

REFERENCES

Amyere M, Revencu N, Helaers R, Pairet E, Baselga E, Cordisco M, et al. Germline loss-of-function mutations in EPHB4 cause a second form of capillary malformation-arteriovenous malformation (CM-AVM2) deregulating RAS-MAPK signaling. Circulation 2017;136:1037−48.

Angulo-Urarte A, Graupera M. When, where and which PIK3CA mutations are pathogenic in congenital disorders. Nat Cardiovasc Res 2022;1:700−14.

Cai R, Gu H, Liu F, Wang L, Zeng X, Yu W, et al. Novel GNAQ mutation(R183G) of Port-wine stains: first case in East Asia. Int J Dermatol 2019;58:e75−7.

Couto JA, Ayturk UM, Konczyk DJ, Goss JA, Huang AY, Hann S, et al. A somatic GNA11 mutation is associated with extremity capillary malformation and overgrowth. Angiogenesis 2017;20:303−6.

Couto JA, Huang L, Vivero MP, Kamitaki N, Maclellan RA, Mulliken JB, et al. Endothelial cells from capillary malformations are enriched for somatic GNAQ mutations. Plast Reconstr Surg 2016;137:77e. −82e.

Cuschieri S. The STROBE guidelines. Saudi J Anaesth 2019;13:S31−4.

Eerola I, Boon LM, Mulliken JB, Burrows PE, Dompmartin A, Watanabe S, et al. Capillary malformation-arteriovenous malformation, a new clinical and genetic disorder caused by RASA1 mutations. Am J Hum Genet 2003;73:1240−9.

Enjolras O, Mulliken JB. The current management of vascular birthmarks. Pediatr Dermatol 1993;10:311−3.

Fjær R, Marciniak K, Sundnes O, Hjorthaug H, Sheng Y, Hammarström C, et al. A novel somatic mutation in GNB2 provides new insights to the pathogenesis of Sturge-Weber syndrome. Hum Mol Genet 2021;30:1919−31.

Geronemus RG, Ashinoff R. The medical necessity of evaluation and treatment of port-wine stains. J Dermatol Surg Oncol 1991;17:76−9.

Goss JA, Konczyk DJ, Smits P, Sudduth CL, Bischoff J, Liang MG, et al. Diffuse capillary malformation with overgrowth contains somatic PIK3CA variants. Clin Genet 2020;97:736−40.

Huang L, Bichsel C, Norris AL, Thorpe J, Pevsner J, Alexandrescu S, et al. Endothelial GNAQ p.R183Q increases ANGPT2 (angiopoietin-2) and drives formation of enlarged blood vessels. Arterioscler Thromb Vasc Biol 2022;42:e27−43.

Huikeshoven M, Koster PH, de Borgie CA, Beek JF, van Gemert MJ, van der Horst CM. Redarkening of port-wine stains 10 years after pulsed-dye-laser treatment. N Engl J Med 2007;356:1235−40.

Jansen P, Müller H, Lodde GC, Zaremba A, Möller I, Sucker A, et al. GNA14, GNA11, and GNAQ mutations are frequent in benign but not malignant cutaneous vascular tumors. Front Genet 2021;12:663272.

Jordan M, Carmignac V, Sorlin A, Kuentz P, Albuisson J, Borradori L, et al. Reverse phenotyping in patients with skin capillary malformations and mosaic GNAQ or GNA11 mutations defines a clinical spectrum with genotype-phenotype correlation. J Invest Dermatol 2020;140:1106−11010.e2.

Kobialka P, Sabata H, Vilalta O, Gouveia L, Angulo-Urarte A, Muixí L, et al. The onset of PI3K-related vascular malformations occurs during angiogenesis and is prevented by the AKT inhibitor miransertib. EMBO Mol Med 2022;14:e15619.

Korff T, Augustin HG. Tensional forces in fibrillar extracellular matrices control directional capillary sprouting. J Cell Sci 1999;112:3249−58.

Lanigan SW, Cotterill JA. Psychological disabilities amongst patients with port wine stains. Br J Dermatol 1989;121:209−15.

Le Cras TD, Goines J, Lakes N, Pastura P, Hammill AM, Adams DM, et al. Constitutively active PIK3CA mutations are expressed by lymphatic and vascular endothelial cells in capillary lymphatic venous malformation. Angiogenesis 2020;23:425−42.

Lee A, Driscoll D, Gloviczki P, Clay R, Shaughnessy W, Stans A. Evaluation and management of pain in patients with Klippel-Trenaunay syndrome: a review. Pediatrics 2005;115:744−9.

Lian CG, Sholl LM, Zakka LR, O TM, Liu C, Xu S, et al. Novel genetic mutations in a sporadic port-wine stain. JAMA Dermatol 2014;150:1336−40.

Masnari O, Landolt MA, Roessler J, Weingaertner SK, Neuhaus K, Meuli M, et al. Self- and parent-perceived stigmatisation in children and adolescents with congenital or acquired facial differences. J Plast Reconstr Aesthet Surg 2012;65:1664−70.

Meijering E, Jacob M, Sarria JC, Steiner P, Hirling H, Unser M. Design and validation of a tool for neurite tracing and analysis in fluorescence microscopy images. Cytometry A 2004;58:167−76.

Mulliken JB, Burrows PE, Fishman SJ. Mulliken and Young's vascular anomalies: hemangiomas and malformations. Oxford, United Kingdom: Oxford University Press; 2013.

Nguyen V, Hochman M, Mihm MC Jr, Nelson JS, Tan W. The pathogenesis of port wine stain and Sturge Weber syndrome: complex interactions between genetic alterations and aberrant MAPK and PI3K activation. Int J Mol Sci 2019;20.

Orlova VV, van den Hil FE, Petrus-Reurer S, Drabsch Y, Ten Dijke P, Mummery CL. Generation, expansion and functional analysis of endothelial cells and pericytes derived from human pluripotent stem cells. Nat Protoc 2014;9:1514−31.

Revencu N, Boon LM, Mendola A, Cordisco MR, Dubois J, Clapuyt P, et al. RASA1 mutations and associated phenotypes in 68 families with capillary malformation-arteriovenous malformation. Hum Mutat 2013;34:1632−41.

Revencu N, Boon LM, Mulliken JB, Enjolras O, Cordisco MR, Burrows PE, et al. Parkes Weber syndrome, vein of Galen aneurysmal malformation, and other fast-flow vascular anomalies are caused by RASA1 mutations. Hum Mutat 2008;29:959−65.

Sasaki M, Jung Y, North P, Elsey J, Choate K, Toussaint MA, et al. Introduction of mutant GNAQ into endothelial cells induces a vascular malformation phenotype with therapeutic response to imatinib. Cancers (Basel) 2022;14:413.

Schneider BV, Mitsuhashi Y, Schnyder UW. Ultrastructural observations in port wine stains. Arch Dermatol Res 1988;280:338–45.

Schrenk S, Bischoff LJ, Goines J, Cai Y, Vemaraju S, Odaka Y, et al. MEK inhibition reduced vascular tumor growth and coagulopathy in a mouse model with hyperactive GNAQ. Nat Commun 2023;14:1929.

Shirley MD, Tang H, Gallione CJ, Baugher JD, Frelin LP, Cohen B, et al. Sturge-Weber syndrome and port-wine stains caused by somatic mutation in GNAQ. N Engl J Med 2013;368:1971–9.

Siegel DH, Cottrell CE, Streicher JL, Schilter KF, Basel DG, Baselga E, et al. Analyzing the genetic spectrum of vascular anomalies with overgrowth via cancer genomics. J Invest Dermatol 2018;138:957–67.

Thomas-Sohl KA, Vaslow DF, Maria BL. Sturge-Weber syndrome: a review. Pediatr Neurol 2004;30:303–10.

Vahidnezhad H, Youssefian L, Uitto J. Klippel-Trenaunay syndrome belongs to the PIK3CA-related overgrowth spectrum (PROS). Exp Dermatol 2016;25:17–9.

van der Stoel M, Schimmel L, Nawaz K, van Stalborch AM, de Haan A, Klaus-Bergmann A, et al. DLC1 is a direct target of activated YAP/TAZ that drives collective migration and sprouting angiogenesis. J Cell Sci 2020;133:jcs239947.

van Drooge AM, Beek JF, van der Veen JP, van der Horst CM, Wolkerstorfer A. Hypertrophy in port-wine stains: prevalence and patient characteristics in a large patient cohort. J Am Acad Dermatol 2012;67:1214–9.

van Raath MI, Chohan S, Wolkerstorfer A, van der Horst CMAM, Storm G, Heger M. Port wine stain treatment outcomes have not improved over the past three decades. J Eur Acad Dermatol Venereol 2019;33:1369–77.

Vila Cuenca M, Cochrane A, van den Hil FE, de Vries AAF, Lesnik Oberstein SAJ, Mummery CL, et al. Engineered 3D vessel-on-chip using hiPSC-derived endothelial- and vascular smooth muscle cells. Stem Cell Rep 2021;16:2159–68.

Supplementary File S1. Gene panel applied for next-generation sequencing

AKT1
AKT2
AKT3
BRAF
FGFR2
FGFR3
GNA11
GNA14
GNAQ
GNAS
HRAS
IDH1
IDH2
KRAS
KRT1
MAP2K1
MTOR
NRAS
PIK3CA
PIK3R2
PTEN
RASA1
TEK